EUROFUSION WPJET1-PR(14) 12548

A S Jacobsen et al.

Velocity-space sensitivity of neutron spectrometry measurements

Preprint of Paper to be submitted for publication in
Nuclear Fusion

This work has been carried out within the framework of the EUROfusion Consortium and has received funding from the Euratom research and training programme 2014-2018 under grant agreement No 633053. The views and opinions expressed herein do not necessarily reflect those of the European Commission.

Velocity-Space Sensitivity of Neutron Spectrometry Measurements

A.S. Jacobsen[1], M. Salewski[1], J. Eriksson[2], G. Ericsson[2], S.B. Korsholm[1], F. Leipold[1], S.K. Nielsen[1], J. Rasmussen[1], M. Stejner[1]
and JET EFDA contributors*

JET-EFDA, Culham Science Centre, OX14 3DB, Abingdon, UK

[1]Association EURATOM–DTU, Technical University of Denmark, Department of Physics, DK-2800 Kgs. Lyngby, Denmark
[2]Association EURATOM–VR, Department of Physics and Astronomy, Uppsala University, Sweden
** See annex of F. Romanelli et al, "Overview of JET Results", (24th IAEA Fusion Energy Conference, San Diego, USA (2012)).*

Preprint of Paper to be submitted for publication in
Nuclear Fusion

ABSTRACT

Neutron emission spectrometry (NES) measures the energies of neutrons produced in fusion reactions. Here we present velocity-space weight functions for NES and neutron yield measurements. Weight functions show the sensitivity as well as the accessible regions in velocity space for a given range of the neutron energy spectrum. Combined with a calculated fast-ion distribution function, they determine the part of the distribution function producing detectable neutrons in a given neutron energy range. Furthermore, we construct a forward model based on weight functions capable of rapidly calculating neutron energy spectra. This forward model can be inverted and could thereby be used to directly measure the fast-ion phase-space distribution functions, possibly in a combination with other fast-ion diagnostics. The presented methods and results can be applied to neutron energy spectra measured by any kind of neutron spectrometer and to any neutron yield measurement.

1. INTRODUCTION

Fast ions in fusion devices play an important role. They are created by ionization of injected energetic neutral particles, by acceleration of ions using ion cyclotron resonance heating or by fusion processes. It is envisaged that the fast ions born in the fusion process will deliver a large part of the heating in an eventual fusion power plant. For this to work, it is critical that the fast ions are sufficiently conned. It has been found that fast ions can be redistributed or expelled by magnetohydrodynamic (MHD) modes. Furthermore, it has been observed that the ions can have an influence on the stability of such modes [1, 2]. Therefore, the study of the behaviour of the fast ions and their interplay with MHD modes in present-day fusion devices is important.

One method to diagnose fast ions in fusion plasmas is by analysing the neutrons created in fusion reactions. The energies of the neutrons depend on the energy released in the fusion reactions as well as the velocities of the reacting ions. Neutron emission spectrometers measure neutron energy spectra and hence are sensitive to the velocity distribution functions of these ions. One such spectrometer is the time-of-flight spectrometer TOFOR at JET [3–10]. TOFOR consists of two sets of detectors placed at a known distance from each other. By measuring the time it takes for the neutrons to travel from the first to the second set of detectors, it is possible to infer information about the neutron energy spectrum. Here we present a general method to relate neutron energy spectra and neutron count measurements to velocity space. Furthermore, we apply our method to neutron energy spectra measured by TOFOR.

In calculations of neutron energy spectra, it is convenient to consider three different contributions to the spectra: the thermal part, the beam-beam part and the beam- target part where the term “beam” refers to fast ions from a neutral beam injector and the term “target” refers to the thermal ions. Here, we only study the beam-target contribution originating from the fusion process between a fast ion and a thermal ion. The beam-target contribution often dominates the spectrum, especially for high neutron energies [3]. Neutrons created in a D-D reaction will have energies around 2.45MeV. However, the neutron energy spectrum can be broadened significantly if one or both ions have high energies. If an ensemble of fast

ions concentrated in a small region in velocity space reacts with thermal ions, the neutron spectra will have a characteristic double-hump shape due of the gyro-motion of the ions [6, 7, 11].

Here we develop weight functions for neutron emission spectrometry (NES) and neutron yield measurements analogous to those for fast-ion D (FIDA) spectroscopy [12–14] and collective Thomson scattering (CTS) [15]. Weight functions show the velocity-space sensitivity for a given energy range of a measured spectrum. So far, weight functions have been applied in four different ways for FIDA and CTS measurements. The simplest application is as an illustration of the region of velocity-space that is accessible by a given part of a measured spectrum and the sensitivity within this region [12–31]. For a given fast-ion distribution function, the product of the weight function and the distribution function shows which ions contribute most to the measurements in the given measurement range [12, 13, 25–31]. By integrating the product of the weight functions and a given distribution function, it is possible to calculate a synthetic spectrum which can then be compared with the measured one. This replaces the traditional forward modelling that is often based on time-consuming Monte Carlo calculations [32–34]. Finally, weight functions are the basic ingredients in the pursuit to extract fast- ion distribution functions directly from measurements using tomographic inversion in velocity-space [15, 32–34].

This paper is organized as follows. In section 2 we derive analytic weight functions for NES and neutron yield measurements. In section 3 we calculate weight functions numerically using an existing forward model. We investigate the effect of various bulk ion temperatures on the velocity-space sensitivity of NES measurements in section 4. Weight functions are used to illustrate the region in velocity space measured by a given part of a neutron spectrum in section 5, and in section 6 we formulate a forward model based on weight functions. In section 7 we discuss perspectives, and conclusions are summarised in section 8.

2. ANALYTIC EXPRESSIONS FOR NEUTRON SPECTROMETRY WEIGHT FUNCTIONS

A fusion process between a fast deuterium beam ion and a thermal deuterium target ion can create a neutron and a Helium-3 ion according to the following reaction:

$$\mathrm{D} + \mathrm{D} \rightarrow {}^{3}\mathrm{He} + \mathrm{n}\,. \tag{1}$$

The neutrons leave the plasma and can be detected using neutron spectrometers. The energies of the detected neutrons depend on the velocities of the reacting ions. Here we show which part of velocity space can generate neutrons with energies in particular energy ranges using weight functions. Weight functions are defined as functions relating a given measurement to the fast-ion phase-space distribution function, $f\left(v_{\parallel}, v_{\perp}, \mathbf{r}\right)$,

$$s\left(v_{n,1}, v_{n,2}, \phi\right) = \int_{vol} \int_{0}^{\infty} \int_{-\infty}^{\infty} w\left(v_{n,1}, v_{n,2}, \phi, v_{\parallel}, v_{\perp}, \mathbf{r}\right) f\left(v_{\parallel}, v_{\perp}, \mathbf{r}\right) \mathrm{d}v_{\parallel} \mathrm{d}v_{\perp} \mathrm{d}\mathbf{r}\,, \tag{2}$$

where $s\,(v_{\mathrm{n},1}, v_{\mathrm{n},2}, \phi)$ is the detection rate of neutrons with velocities between $v_{\mathrm{n},1}$ and $v_{\mathrm{n},2}$ measured by a detector at an angle ϕ between its line-of-sight and the magnetic field. $(v_{\mathrm{n},1}, v_{\mathrm{n},2}, \phi, v_{\parallel}, v_{\perp}, \mathbf{r})$ is the weight function in units of $\left[\frac{\mathrm{N}_n}{\mathrm{sN}_f}\right]$, i.e. number of detected neutrons in a given energy or velocity range per second per fast ion. $f\,(v_{\parallel}, v_{\perp}, \mathbf{r})$ is in units of $\left[\frac{\mathrm{N}_f \mathrm{n}^2}{\mathrm{m}^5}\right]$. $v_{\parallel}$ and $v_{\perp}$ denote the ion velocity parallel and perpendicular to the magnetic field, respectively, and $\mathbf{r}$ denotes the spatial coordinates. $v_{\parallel}$ is defined positive in the co-current direction, which is usually in the direction opposite to the magnetic field. The spatial integral is over the conical measurement volume oriented along the line-of-sight. The fast-ion phase-space distribution function and the weight functions have a spatial dependence since the plasma parameters may vary significantly along the line-of-sight. Equation (2) can also be expressed as a function of energy and pitch

$$s\,(E_{n,1}, E_{n,2}, \phi) = \int\int\int w\,(E_{n,1}, E_{n,2}, \phi, E, p, \mathbf{r})\, f\,(E, p, \mathbf{r})\ \mathrm{d}E\,\mathrm{d}p\,\mathrm{d}\mathbf{r}\,, \tag{3}$$

where E is the fast-ion energy, p is the pitch defined as $p = {}^{v_{\parallel}}/_{v}$ and E_n is the neutron energy. In the following, weight functions will be derived in $(v_{\parallel}, v_{\perp})$-space as the mathematical expressions take a simpler form in these coordinates. However, the most important expressions will be given in the more commonly used (E, p)-space as well. Weight functions can be written as a product of two factors:

$$w\left(v_{n,1}, v_{n,2}, \phi, v_{\parallel}, v_{\perp}, \mathbf{r}\right) = R\left(\phi, v_{\parallel}, v_{\perp}, \mathbf{r}\right) \mathrm{prob}\left(v_{n,1} < v_n < v_{n,2} \middle| \phi, v_{\parallel}, v_{\perp}\right)\,. \tag{4}$$

prob $(v_{n,1} < v_n < v_{n,2} \mid \phi, v_{\parallel}, v_{\perp})$ is the probability that a neutron has a velocity between $v_{n,1}$ and $v_{n,2}$ (or likewise a kinetic energy between $E_{n,1}$ and $E_{n,2}$), given it was created in a fusion reaction between a thermal ion and a fast ion with velocity $(v_{\parallel}, v_{\perp})$ and observed at an angle ϕ. The conditioning symbol "$\mid$" means given. This factor contains the spectral information that determines which part of velocity space a given interval in the neutron energy spectrum is susceptible to. R $(\phi, v_{\parallel}, v_{\perp}, \mathbf{r})$ is the rate of detected neutrons per fast ion as a function of velocity and position.

Before we derive analytic expressions for the probability part, we illustrate the properties of the rate function R $(\phi, v_{\parallel}, v_{\perp}, \mathbf{r})$. The rate function gives the total number of neutrons detected per second per fast ion irrespective of the neutron energies. It depends on the relative velocity, $\mathbf{v}_{rel}$ between the fast and thermal ions and can be calculated according to

$$R\left(\phi, v_{\parallel}, v_{\perp}, \mathbf{r}\right) = \frac{\Omega\,(\mathbf{r})}{4\pi} \int\int f_t\left(v_{t,\parallel}, v_{t,\perp}, \mathbf{r}\right) \sigma\,(\phi, v_{rel})\, v_{rel}\,\mathrm{d}v_{t,\parallel}\mathrm{d}v_{t,\perp}\,, \tag{5}$$

where Ω is the solid-angle of the detector as seen from the plasma as a function of position, f_t is the thermal ion distribution function, $v_{t,\parallel}$ and $v_{t,\perp}$ are the thermal ion velocities parallel and perpendicular to the magnetic field, σ is the fusion cross section and $v_{rel} = \mid v_{rel} \mid$ is the magnitude of the relative velocity. The integral is over the thermal ion velocity and is calculated by numerically sampling over a Maxwellian distribution.

Here we illustrate some basic properties of R by assuming that the velocities of the fast ions are significantly higher than the velocities of the thermal ions. Furthermore we neglect the ϕ-dependence of the cross section and the finite solid-angle. This allows us to approximate the thermal-ion distribution function by a δ-function located at origo. In this case, the relative velocity becomes the velocity of the fast ions and equation (5) reduces to

$$R\left(v_{\parallel}, v_{\perp}, \mathbf{r}\right) = n_t\left(\mathbf{r}\right)\sigma\left(\sqrt{v_{\parallel}^2 + v_{\perp}^2}\right)\sqrt{v_{\parallel}^2 + v_{\perp}^2}\,, \tag{6}$$

where n_t is the thermal ion density. In this case R does not depend on pitch as shown in figure 1(a). Here, σ is approximated by [35]

$$\sigma = \frac{S}{E_{cm}\left(\exp\left(\frac{B_G}{\sqrt{E_{cm}}}\right) - 1\right)}\,, \tag{7}$$

where E_{cm} is the energy in the center-of-mass frame, B_G is a constant and S is a fifth-order polynomial in E_{cm}. A thermal ion density of $5{\times}10^{19}$ m^{-3} is used. A drifting thermal target distribution modelled as a δ-function located at a non-zero parallel velocity and no perpendicular velocity gives a rate function of

$$R\left(v_{\parallel}, v_{\perp}, \mathbf{r}\right) = n_t\left(\mathbf{r}\right)\sigma\left(\sqrt{\left(v_{\parallel} - v_d\right)^2 + v_{\perp}^2}\right)\sqrt{\left(v_{\parallel} - v_d\right)^2 + v_{\perp}^2} \tag{8}$$

where v_d is the drift velocity parallel to the magnetic field. This introduces an asymmetry in pitch, as we show in figure 1(b). Here a co-current drift velocity of $v_d = 2.1{\times}10^5$ m/s is used. In this situation, the neutron rate is largest for fast ions with negative pitch, as they move in the direction opposite to the thermal drift and thus have a larger relative velocity.

The rate function, R, is the weight function for neutron yield measurements [12], which count any neutron irrespective of energy. This follows from equation (4) for $v_{n,1} \to -\infty$ and $v_{n,2} \to -\infty$ as the probability function becomes unity for very large neutron energy ranges, i.e. the probability that a detected neutron has a velocity between $\pm\infty$ must be 1. Neutron count measurements are most sensitive in the velocity- space regions with the largest amplitudes of R, where most neutrons are produced per ion per second.

Now we derive analytic expressions for the probability part of the weight functions. The probability that a detected neutron has a velocity in a given interval, $v_{n,1} < v_n < v_{n,2}$ is the integral of the probability density function of the neutron velocity integrated over this interval:

$$\mathrm{prob}\left(v_{n,1} < v_n < v_{n,2}\,\middle|\,\phi, v_{\parallel}, v_{\perp}\right) = \int_{v_{n,1}}^{v_{n,2}} pdf_{v_n}\,\mathrm{d}v_n\,. \tag{9}$$

We assume that the energy and momentum of the thermal target ions are negligible compared with the energy and momentum of the beam ions, respectively. Thus, given the parallel and perpendicular velocities of the fast ion and the angle, ϕ, to the detector, the neutron velocity only depends on

the gyro-angle, γ, of the fast ion before the reaction [36]. The neutron velocity probability density function can therefore be expressed as a function of the gyro-angle probability density function:

$$pdf_{v_n} = pdf_\gamma \left| \frac{\mathrm{d}\gamma}{\mathrm{d}v_n} \right| . \tag{10}$$

The gyro-angle probability distribution function is assumed uniform:

$$pdf_\gamma = \frac{1}{2\pi} , \tag{11}$$

and the problem reduces to expressing the relation between the gyro-angle of the fast ion and the neutron velocity in known quantities. Conservation of energy during a fusion process between a fast beam ion and a stationary target ion in the lab frame of reference dictates

$$\frac{1}{2} m_f v_f^2 + Q = \frac{1}{2} m_{He} v_{He}^2 + \frac{1}{2} m_n v_n^2 , \tag{12}$$

where m_f, m_{He} and m_n and v_f, v_{He} and v_n are the masses and velocities of the fast ion, the helium ion and the neutron, respectively, and Q is the energy released in the fusion process. For a D-D reaction, Q = 3.27MeV. Conservation of momentum dictates

$$m_f \mathbf{v}_f = m_{He} \mathbf{v}_{He} + m_n \mathbf{v}_n . \tag{13}$$

Isolating v_{He} and squaring gives

$$v_{He}^2 = \frac{1}{m_{He}^2} \left(m_f \mathbf{v}_f - m_n \mathbf{v}_n \right)^2 = \frac{1}{m_{He}^2} \left(m_f^2 v_f^2 + m_n^2 v_n^2 - 2 m_f m_n \mathbf{v}_f \cdot \mathbf{v}_n \right) . \tag{14}$$

To calculate the dot product $v_f \cdot v_n$, we write

$$\mathbf{v}_n = \hat{\mathbf{v}}_n v_n , \tag{15}$$

where $\hat{\mathbf{v}}_n$ is the unit vector in the direction towards the spectrometer along the line-of-sight. The projection of the fast-ion velocity in the direction towards the neutron spectrometer, u, can then be expressed as

$$u = \mathbf{v}_f \cdot \hat{\mathbf{v}}_n . \tag{16}$$

Inserting equations (14), (15) and (16) in equation (12) and isolating u gives

$$u = \frac{1}{2} \frac{(m_{He} + m_n)}{m_f} v_n - \frac{1}{2} \frac{(m_{He} - m_f)}{m_n} \frac{v_f^2}{v_n} - \frac{m_{He}}{m_f m_n} \frac{Q}{v_n} . \tag{17}$$

Only neutrons moving along the line-of-sight towards the neutron spectrometer are detected. We define a ($v_\parallel$, $v_{\perp,1}$, $v_{\perp,2}$)–coordinate system similar to the one defined in reference [15]. The $v_{\perp,1}$-axis

is oriented such that the line-of-sight of the spectrometer lies in the ($v_{\parallel}$, $v_{\perp,1}$)-plane. The fast-ion velocity can be written as

$$\mathbf{v}_f = v_{\parallel}\hat{\mathbf{v}}_{\parallel} + v_{\perp}\cos(\gamma)\,\hat{\mathbf{v}}_{\perp,1} + v_{\perp}\sin(\gamma)\,\hat{\mathbf{v}}_{\perp,2}\,, \tag{18}$$

where $\hat{\mathrm{v}}_{\parallel}$, $\hat{\mathrm{v}}_{\perp,1}$ and $\hat{\mathrm{v}}_{\perp,2}$ are the three unit vectors. In this coordinate system $\hat{\mathrm{v}}_n$ becomes

$$\hat{\mathbf{v}}_n = \cos(\phi)\,\hat{\mathbf{v}}_{\parallel} + \sin(\phi)\,\hat{\mathbf{v}}_{\perp,1}\,. \tag{19}$$

The projected fast-ion velocity, u, can be expressed in terms of the parallel and perpendicular ion velocities [15]:

$$u = \mathbf{v}_f \cdot \hat{\mathbf{v}}_n = v_{\parallel}\cos(\phi) + v_{\perp}\sin(\phi)\cos(\gamma)\ . \tag{20}$$

If, for a given u, equation (20) is fullfilled for γ, then so it is for $2\pi-\gamma$ as well. Combining equations (17) and (20) and isolating γ gives

$$\begin{aligned}\gamma =&\ \arccos\left(\frac{u - v_{\parallel}\cos(\phi)}{v_{\perp}\sin(\phi)}\right)\\ =&\ \arccos\left(\frac{1}{v_{\perp}\sin(\phi)}\left(\frac{1}{2}\frac{(m_{He}+m_n)}{m_f}v_n - \frac{1}{2}\frac{(m_{He}-m_f)}{m_n}\frac{\left(v_{\parallel}^2+v_{\perp}^2\right)}{v_n}\right.\right.\\ &\left.\left. - \frac{m_{He}}{m_f m_n}\frac{Q}{v_n} - v_{\parallel}\cos(\phi)\right)\right)\ .\end{aligned} \tag{21}$$

To find pdf_{vn} from equation (10), we differentiate γ with respect to the neutron velocity

$$\begin{aligned}\frac{\mathrm{d}\gamma}{\mathrm{d}v_n} =& -\frac{1}{\sin(\gamma)}\left(\frac{1}{v_{\perp}\sin(\phi)}\left(\frac{1}{2}\frac{(m_{He}+m_n)}{m_f} + \frac{1}{2}\frac{(m_{He}-m_f)}{m_n}\frac{\left(v_{\parallel}^2+v_{\perp}^2\right)}{v_n^2}\right.\right.\\ &\left.\left. + \frac{m_{He}}{m_f m_n}\frac{Q}{v_n^2}\right)\right)\ .\end{aligned} \tag{22}$$

Combining equations (9)-(11) and changing the integration variable to gives

$$\begin{aligned}\mathrm{prob}\left(v_{n,1} < v_n < v_{n,2}\,\middle|\,\phi, v_{\parallel}, v_{\perp}\right) =&\ \int_{\gamma(v_{n,1})}^{\gamma(v_{n,2})}\frac{1}{2\pi}\frac{\left|\frac{\mathrm{d}\gamma}{\mathrm{d}v_n}\right|}{\frac{\mathrm{d}\gamma}{\mathrm{d}v_n}}\,\mathrm{d}\gamma\\ &+\int_{2\pi-\gamma(v_{n,1})}^{2\pi-\gamma(v_{n,2})}\frac{1}{2\pi}\frac{\left|\frac{\mathrm{d}\gamma}{\mathrm{d}v_n}\right|}{\frac{\mathrm{d}\gamma}{\mathrm{d}v_n}}\,\mathrm{d}\gamma\,.\end{aligned} \tag{23}$$

The second integral in equation (23) arises since equation (20) is fulfilled for both γ and $2\pi - \gamma$ as mentioned earlier. As ϕ is only defined between 0^o and 180^o, the terms in the parenthesis in equation (22) are always positive, and thus the signs of the integrands in equation (23) depend only on γ. For $0 < \gamma < \pi$ the integrand is negative, and for $\pi < \gamma < 2\pi$, the integrand is positive. The probability can now be calculated

$$\begin{aligned} \text{prob}\left(v_{n,1} < v_n < v_{n,2} \left| \phi, v_\parallel, v_\perp \right.\right) &= \frac{1}{2\pi}\left(\int_{\gamma(v_{n,1})}^{\gamma(v_{n,2})} (-1)\,\mathrm{d}\gamma + \int_{2\pi-\gamma(v_{n,1})}^{2\pi-\gamma(v_{n,2})} \mathrm{d}\gamma\right) \\ &= \frac{\gamma\left(v_{n,1}\right) - \gamma\left(v_{n,2}\right)}{\pi}, \end{aligned} \tag{24}$$

where the γ values are given by equation (21). Thus, the probability function is the fraction of the gyroorbit that leads to neutrons with energies within the given neutron energy range. These results are valid for $\phi \neq 0^o$ or 180^o. For $\phi = 0^o$ or 180^o, the projected fast-ion velocity become $v_\parallel$, and a given ($v_\parallel$,$v_\perp$) -coordinate will give a single neutron velocity through equation (17). In this specific case, the probability functions becomes semicircular arcs in ($v_\parallel$,$v_\perp$)-space with values 1. As stated earlier, the probability function can also be expressed in terms of the neutron energy, E_n:

$$\text{prob}\left(E_{n,1} < E_n < E_{n,2} \left| \phi, v_\parallel, v_\perp \right.\right) = \frac{\gamma\left(E_{n,1}\right) - \gamma\left(E_{n,2}\right)}{\pi}. \tag{25}$$

$\gamma\ (E_n)$ is found be inserting $v_n = \sqrt{\frac{2E_n}{m_n}}$ in equation (21). The probability can also be expressed in energy-pitch coordinates.

$$\text{prob}\left(E_{n,1} < E_n < E_{n,2} \left| \phi, E, p \right.\right) = \frac{\gamma\left(E_{n,1}\right) - \gamma\left(E_{n,2}\right)}{\pi}. \tag{26}$$

The values are then calculated from

$$\begin{aligned} \gamma = \arccos\Bigg(\frac{1}{\sqrt{1-p^2}}\frac{1}{\sin(\phi)}\Bigg(&\frac{1}{2}\frac{(m_{He}+m_n)}{\sqrt{m_f m_n}}\sqrt{\frac{E_n}{E}} \\ &- \frac{1}{2}\frac{(m_{He}-m_f)}{\sqrt{m_f m_n}}\sqrt{\frac{E}{E_n}} - \frac{1}{2}\frac{m_{He}}{\sqrt{m_f m_n}}\frac{Q}{\sqrt{E E_n}} - p\cos(\phi)\Bigg)\Bigg). \end{aligned} \tag{27}$$

For the special case $m_{He} = 3m_n$ and $m_f = 2m_n$, which we treat here, equations (17), (21) and (27) reduce considerably. Equation (17) becomes

$$u = v_n - \frac{1}{2}\frac{v_f^2}{v_n} - \frac{3}{2}\frac{Q}{m_n v_n}. \tag{28}$$

Equation (21) becomes

$$\gamma = \arccos\left(\frac{1}{v_\perp \sin(\phi)}\left(v_n - \frac{1}{2}\frac{\left(v_\parallel^2 + v_\perp^2\right)}{v_n} - \frac{3}{2}\frac{Q}{m_n v_n} - v_\parallel \cos(\phi)\right)\right) \tag{29}$$

and equation (27) becomes

$$\gamma = \arccos\left(\frac{1}{\sqrt{1-p^2}\sin(\phi)}\left(\sqrt{2\frac{E_n}{E}} - \frac{1}{2}\sqrt{\frac{E}{2E_n}} - \frac{3}{2}\frac{Q}{\sqrt{2EE_n}} - p\cos(\phi)\right)\right). \tag{30}$$

Examples of probabilities calculated using equation (25) for ϕ = 90°, 45° and 10° for different neutron energies are plotted in figure 2 ($v_{\|}$,$v_{\perp}$)–space. They are calculated for a neutron energy interval of $\Delta E_n = E_{n,2} - E_{n,1}$ = 0.1MeV. The coloured regions are observable for the given neutron energy range and projection angle whereas the white regions cannot contribute to the signal and are unobservable regions. The probability functions corresponding to different neutron energy ranges cover different regions in velocity space. We have chosen to show these examples of the weight functions for very large ($v_{\|}$,$v_{\perp}$)–values in order to reveal the shape of the observable region. Fast ions at JET typically have lower energies. Figure 2 shows that the weight functions for higher neutron energies cover larger velocity-space regions. The observable regions for a given neutron energy do not necessarily include the regions for lower neutron energies as demonstrated by figures 2(g) and 2(i). The probability for the neutrons to be in a particular energy range is largest for ions close to the edges of the probability functions. This is analogous to weight functions for CTS and FIDA [14, 15].

The limiting edges separating the observable region in velocity space from the unobservable region, i.e. the edges of the weight functions, can be found be inserting cos (γ) = 1 in equation (21), as in this case the projected velocities and therefore the neutron energies are at their extreme values. In this case, equation (21) can be rewritten in the form $(v_{\|} - v_{\|,0})^2 + (v_{\perp} - v_{\perp,0})^2 = r^2$ which is the equation of a circle centred at $(v_{\|,0} - v_{\perp,0})^2$ with radius r. Rewriting equation (21) with cos (γ) = –1 gives

$$v_{\|,0} = -\frac{\cos(\phi)}{m_{He} - m_f} m_n v_n\,, \tag{31}$$

$$v_{\perp,0} = \frac{\sin(\phi)}{m_{He} - m_f} m_n v_n\,, \tag{32}$$

$$r = \sqrt{2\frac{m_{He}(m_{He} + m_n - m_f)}{m_f(m_{He} - m_f)^2}E_n - 2\frac{m_{He}}{m_f(m_{He} - m_f)}Q}\,. \tag{33}$$

The center of the circle lies on a straight line through the origin with angle 180° – ϕ to the $v_{\|}$–axis since $\frac{v_{\perp,0}}{v_{\|,0}}$ = –tan (ϕ). The distance from the center of the circle to the origin is. Thus, the larger the neutron energy, the further the center of the weight functions moves away from the origin. Rewriting equation (21) with cos (γ) = 1 gives

$$v'_{\|,0} = v_{\|,0} \tag{34}$$

$$v'_{\perp,0} = -v_{\perp,0} \tag{35}$$

$$r' = r\,, \tag{36}$$

where $(v'_{\|,0} - v'_{\perp,0})^2$ and r′ are the center coordinates and radius of a second circle. Thus the second circle is a mirror image of the first, mirrored across the $v_{\|}$-axis. The weight functions are bounded by the parts of the circles with positive $v_{\perp}$-coordinates. This differs from weight functions for FIDA and CTS which have characteristic triangular shapes in $(v_{\|,0} - v_{\perp,0})$ -coordinates [14, 15]. Letting $r \rightarrow 0$ in equation (33) gives a lower limit for the neutron energy E_n. For D-D neutrons this limit is found to be $E_n = {}^{Q}/_{2}$. Figure 2 further shows the dependence of the weight functions on the projection angle ϕ. The weight functions occupy a smaller region of velocity-space for ϕ-angles far from 90°, a behaviour also seen for CTS and FIDA weight functions. For a perpendicular view ($\phi = 90^{o}$), the weight functions are symmetric with respect to $v_{\|}$ as figures 2(a), 2(b) and 2(c) show. This is also evident from equation (31) as $v_{\|,0} = 0$ for $\phi = 90^{o}$. For $0^{o} < \phi < 90^{o}$ the weight functions are shifted towards negative parallel velocities, whereas for $90^{o} < \phi < 180^{o}$ they are shifted towards positive parallel velocities.

Figure 3 shows examples of the probability functions calculated in (E,p)-space. We again calculate the probability functions up to high ion energies to show large portions of the weight functions. As for $(v_{\|,0} - v_{\perp,0})$–coordinates, we find that for smaller angles, the weight functions cover a smaller region of (E, p)-space, and the symmetry in pitch for $\phi = 90^{o}$ is evident. However, the shape of the weight functions in (E, p)-space is more complicated than in $(v_{\|} - v_{\perp})$-space. The probability functions have finite values down to $E = 0$MeV for $E_n \simeq 2.45$MeV. However, this does not mean that the full weight functions have significant values at very low ion energies, as the rate function goes rapidly to zero for such low ion energies.

3. NUMERICAL CALCULATION OF NEUTRON SPECTROMETRY WEIGHT FUNCTIONS

Weight functions can be computed numerically using a forward model capable of calculating a neutron energy spectrum for a given arbitrary beam-ion velocity distribution and a given thermal ion velocity distribution function. The forward model used here has previously been used for neutron spectrometry analysis in e.g. [8, 37]. We define a point-like velocity distribution function for the fast ions and calculate the corresponding energy spectrum. This distribution function can be written as a product of -functions

$$f\,(E, p, \mathbf{r}) = N_f \delta\,(E_0 - E)\,\delta\,(p_0 - p)\,\delta\,(\mathbf{r}_0 - \mathbf{r})\ , \tag{37}$$

where N_f is the number of fast ions. Inserting equation (37) in equation (3) and integrating gives the amplitude of the weight function at $(E_0, p_0, \mathbf{r}_0)$ for the given neutron energy range and projection angle:

$$w\left(E_{n,1}, E_{n,2}, \phi, E_0, p_0, \mathbf{r}_0\right) = \frac{s\left(E_{n,1}, E_{n,2}, \phi\right)}{N_f} \,. \tag{38}$$

The probability part can now be calculated

$$\text{prop}\left(E_{n,1} < E_n < E_{n,2} | \, \phi, E_0, p_0\right) = \frac{w\left(E_{n,1}, E_{n,2}, \phi, E_0, p_0, \mathbf{r}_0\right)}{R\left(\phi, E_0, p_0, \mathbf{r}_0\right)} \,. \tag{39}$$

where the rate part can be calculated using equation (5) or directly from the spectrum as

$$R\left(\phi, E_0, p_0, \mathbf{r}_0\right) = \frac{1}{N_f} \int_0^\infty s\left(E_n, \phi\right) \mathrm{d}E_n \,. \tag{40}$$

This is repeated on a numerical grid of velocity-space positions of the point-like distribution. Figure 4 compares examples of the probability part of the weight functions calculated using the analytical approach derived in section 2 and the numerical approach calculated using equation (39). The analytic and numeric results agree very well, in shape as well as in amplitudes. The numerically calculated weight functions are less smooth than the analytic ones since the forward model uses a Monte Carlo approach. Furthermore, the numerical weight functions have a coarser velocity-space resolution because the computation of analytic weight functions requires much less computational time.

4. EFFECT OF TEMPERATURE ON THE VELOCITY-SPACE SENSITIVITY

Our approach to calculate analytic weight functions assumed stationary target ions corresponding to zero temperature of the thermal ion distribution. We can readily investigate the effect of a non-zero temperature on the velocity-space sensitivity using numerical weight functions. The effect of increasing the temperature of the Maxwellian target distribution is shown in figure 5. The sharp features of the zero temperature probability function are being blurred for a finite temperature of the target distribution. The larger the temperature, the more blurred the probability functions become. The maximum close to the edge of the probability function is reduced and broadened already for a temperature of 1keV. The probability function covers a slightly larger velocity- space region. These trends become more pronounced with increasing temperatures. The weight functions become blurred because the thermal ions have a Maxwellian distribution. Hence fast ions with given ($v_{\|}$, $v_{\perp}$)–coordinates and gyroangles produce neutrons with energies that are distributed with a similarly broadened Maxwellian distribution. The black lines in figure 5 show the edge of the weight function in the T = 0keV case calculated using equations (31)–(33) and transformed to (E, p)–space.

5. WEIGHT FUNCTIONS USED TO SHOW INTERROGATION REGIONS

For the remainder of this paper, we will consider the complete weight functions consisting of the probability part and the neutron rate part according to equation (4). We will be using numerical weight functions calculated using appropriate angle-dependant cross sections and plasma parameters. As mentioned earlier, a weight function shows the velocity-space sensitivity of the measurement for

a given neutron energy range and in particular which regions are accessible by the measurements. Figure 6(a) shows a measured time-of-flight spectrum from TOFOR measured during JET Pulse No: 68138 together with a synthetic time-of-flight spectrum from a calculated energy-spectrum.

The corresponding synthetic neutron energy spectrum is shown in figure 6(b). A shaded bar has been inserted in figure 6(b). The weight function for the energies corresponding to the shaded interval is shown in figure 6(c), i.e. the neutrons with energies in the shaded region of figure 6(b) can only arise from reactions involving fast ions with velocities located in the coloured region of figure 6(c). This weight function is calculated using a background ion temperature of 2.3keV. Furthermore, it is possible to estimate which regions in velocity space generate most neutrons for a given velocity- space distribution function. To do this one plots the product of a weight function and the distribution function, i.e. the integrand of equations (2) or (3). The integrand shows the number density of detected neutrons with energies in a given energy range per second in velocity space for the particular distribution function. The fast-ion distribution function has been calculated using TRANSP with the NUBEAM module [38] for JET Pulse No: 68138. The fast ions have been simulated in the entire TOFOR measurement volume. Here the velocity distribution of the ions in the center of JET is considered, as these will often produce most of the detected neutrons. The product of the weight function and the central fast ion velocity distribution function is shown in figure 6(d).

Plotting a calculated fast-ion distribution function together with a weight function illustrates the part of the distribution function that is measurable in the given part of the neutron energy spectrum as well as the sensitivity. Examples are shown in figures 7(a) and 7(b). The fast-ion distribution functions are shown as black contour lines, and the weight function is shown in colours. The weight function is calculated for $E_n = 2.3 \pm 0.015$MeV, $\phi = 90^o$ and $E_{thermal} = 2$keV. Figure 7(a) shows a beam-ion slowing down distribution function originating from an off-axis radial injection, while figure 7(b) shows a distribution function from an on-axis tangential injection. Both are from JET Pulse No: 69242.

The products of the weight function and the distribution functions are shown in figures 7(c) and 7(d). In the case of a normal injection, the range of neutron energies between 2.285MeV and 2.315MeV measures fast ions with energies higher than 40keV and pitch values between –0.75 and 0.75 as seen in figure 7(c). For a tangential injection, most detected neutrons are produced in reactions involving passing ions with $p > 0.5$ as seen in figure 7(d).

6. WEIGHT FUNCTIONS USED IN A FORWARD MODEL

Weight functions can be used to calculate a spectrum given a fast-ion distribution function, $f(E, p, \mathbf{r})$, using equation (3). This is done by evaluating equation (3) for every neutron energy interval of relevance. Both the fast-ion distribution function and the weight function have a spatial dependence as the ion temperatures and densities can vary throughout the acceptance cone of the neutron detector. Figure 8 shows neutron energy spectra calculated with a conventional forward model and

using weight functions. The two methods produce spectra that are almost identical. The spectrum computed using weight functions is calculated by splitting the entire TOFOR viewing cone up in 10 volumes. In each volume, the ion temperatures and densities are assumed constant and a fast-ion distribution function is simulated for each. Once the weight functions have been calculated, the weight function method is significantly faster than the traditional forward model since the spectra can be calculated by matrix multiplication. This is advantageous if synthetic spectra for many different fast-ion distribution functions are to be calculated.

7. DISCUSSION

Recent studies have investigated the potential of combining measurements taken simultaneously using several fast-ion D_α or collective Thomson scattering views, and even combining measurements from the two different types of diagnostics [32, 33]. This is made possible by the use of weight functions in the form of equation (2) in tomographic inversion algorithms to directly measure the fast-ion distribution function. NES weight functions as we formulated here allow us to combine NES measurements with CTS and FIDA measurements to measure the fast-ion distribution function. However, so far only localized measurements in small measurement volumes such as those for CTS or FIDA can be combined whereas the measurement volume of NES is a cone oriented along the line-of-sight. The larger measurement volume makes a combination cumbersome but not impossible. Assuming that most detectable neutrons have been produced near the plasma center, and assuming that the beam-target contribution dominates, NES measurements could be combined with CTS or FIDA measurements from central measurement volumes. No further development of the NES weight functions are needed under these assumptions. Otherwise, the inference of the fast-ion distribution function must account for the spatial dependencies.

The examples shown in this paper have been calculated using values of the $d(d,n)^3He$ reaction. However, the derivation in section 2 is also valid, under the assumptions given, for neutrons from the $d(t,n)^4He$ reaction, or any other reaction, as long as the appropriate values of m_f, m_{He} and Q are used.

CONCLUSIONS

We have calculated velocity-space weight functions for neutron spectrometers and neutron yield counters both analytically and numerically, considering the often dominant beam-target reaction. These show the velocity-space sensitivity of NES measurements in given energy ranges of detected neutrons. The accessible region in $(v_\parallel, v_\perp)$–space is bounded by circles or circular arcs in the limit where the velocities of the target ions are zero. The closer a fast ion is to the edge of the circle, the more likely it is to generate a detectable neutron in the given energy range. The larger the energy of the detected neutron, the larger the observation region becomes for a given observation angle. Finite temperatures of the thermal target ions blur the weight functions. The weight functions can be used to investigate the region in velocity-space accessible by a given part of a neutron spectrum.

Given a fast-ion distribution function, the weight functions can be used to calculate the part of the distribution function that generates most neutrons in the given energy range. Furthermore, they can be used in a forward model based on matrix multiplication that is significantly faster than traditional forward models based on Monte Carlo sampling.

ACKNOWLEDGEMENTS

This work, supported by the European Communities under the contract of Association between Euratom and DTU, was partly carried out within the framework of the European Fusion Development Agreement. The views and opinions expressed herein do not necessarily reflect those of the European Commission.

REFERENCES

[1]. W.W. Heidbrink and G.J. Sadler. The behaviour of fast ions in tokamak experiments. Nuclear Fusion, **34**(4):535–615, 1994.

[2]. S.D. Pinches, H.L. Berk, D.N. Borba, B.N. Breizman, S. Briguglio, A. Fasoli, G. Fogaccia, M.P. Gryaznevich, V. Kiptily, M.J. Mantsinen, S.E. Sharapov, D. Testa, R.G.L Vann, G. Vlad, F. Zonca, and JET-EFDA Contributors. The role of energetic particles in fusion plasmas. Plasma Physics and Controlled Fusion, **46**(12B):B187–B200, December 2004.

[3]. M. Gatu Johnson, L. Giacomelli, A. Hjalmarsson, J. Källne, M. Weiszflog, E. Andersson Sunden, S. Conroy, G. Ericsson, C. Hellesen, E. Ronchi, H. Sjöstrand, G. Gorini, M. Tardocchi, A. Combo, N. Cruz, J. Sousa, and S. Popovichev. The 2.5-MeV neutron time-of- ight spectrometer TOFOR for experiments at JET. Nuclear Instruments and Methods in Physics Research Section A: Accelerators, Spectrometers, Detectors and Associated Equipment, **591**(2):417–430, June 2008.

[4]. M. Gatu Johnson, C. Hellesen, E. Andersson Sunden, M. Cecconello, S. Conroy, G. Ericsson, G. Gorini, V. Kiptily, M. Nocente, S. Pinches, E. Ronchi, S. Sharapov, H. Sjöstrand, M. Tardocchi, and M. Weiszog. Neutron emission from beryllium reactions in JET deuterium plasmas with 3 He minority. Nuclear Fusion, **50**(4):045005, April 2010.

[5]. M. Gatu Johnson, S. Conroy, M Cecconello, E. Andersson Sunden, G. Ericsson, M. Gherendi, C. Hellesen, A. Hjalmarsson, A. Murari, S. Popovichev, E. Ronchi, M Weiszflog, and V.L. Zoita. Modelling and TOFOR measurements of scattered neutrons at JET. Plasma Physics and Controlled Fusion, **52**(8):085002, August 2010.

[6]. C. Hellesen, M. Gatu Johnson, E. Anderson Sunden, S. Conroy, G. Ericsson, E Ronchi, H. Sjöstrand, M. Weiszflog, G. Gorini, M. Tardocchi, T. Johnson, V.G. Kiptily, S.D. Pinches, and S.E. Sharapov. Neutron emission generated by fast deuterons accelerated with ion cyclotron heating at JET. Nuclear Fusion, **50**(2):022001, February 2010.

[7]. C. Hellesen, M. Gatu Johnson, E. Andersson Sunden, S. Conroy, G. Ericsson, J. Eriksson, G. Gorini, T. Johnson, V.G. Kiptily, S.D. Pinches, S.E. Sharapov, H. Sjöstrand, M. Nocente, M. Tardocchi, and M. Weiszflog. Measurements of fast ions and their interactions with MHD

activity using neutron emission spectroscopy. Nuclear Fusion, **50**(8):084006, August 2010.

[8]. C. Hellesen, M. Albergante, E. Andersson Sunden, L. Ballabio, S. Conroy, G. Ericsson, M. Gatu Johnsson, L. Giacomelli, G. Gorini, A. Hjalmarsson, I. Jenkins, J Källne, E. Ronchi, H. Sjöstrand, M. Tardocchi, I. Voitsekhovitch, and M. Weiszflog. Neutron spectroscopy measurements and modeling of neutral beam heating fast ion dynamics. Plasma Physics and Controlled Fusion, **52**(8):085013, August 2010.

[9]. C. Hellesen, M. Gatu Johnson, E. Andersson Sunden, S. Conroy, G. Ericsson, J. Eriksson, H. Sjöstrand, M. Weiszflog, T. Johnson, G. Gorini, M. Nocente, M. Tardocchi, V.G. Kiptily, S.D. Pinches, and S.E. Sharapov. Fast-ion distributions from third harmonic ICRF heating studied with neutron emission spectroscopy. Nuclear Fusion, **53**(11):113009, November 2013.

[10]. J. Eriksson, C. Hellesen, E. Andersson Sunden, M. Cecconello, S. Conroy, G. Ericsson, M. Gatu Johnson, S.D. Pinches, S.E. Sharapov, and M. Weiszflog. Finite Larmor radii eects in fast ion measurements with neutron emission spectrometry. Plasma Physics and Controlled Fusion, **55**(1):015008, January 2013.

[11]. W.W. Heidbrink. Fusion reaction spectra produced by anisotropic ^{3}He ions during ICRF. Nuclear Fusion, **24**(5):636{639, 1984.

[12]. W.W. Heidbrink, Y. Luo, K.H. Burrell, R.W. Harvey, R.I. Pinsker, and E. Ruskov. Measurements of fast-ion acceleration at cyclotron harmonics using Balmer-alpha spectroscopy. Plasma Physics and Controlled Fusion, **49**(9):1457{1475, September 2007.

[13]. W W Heidbrink. Fast-ion D measurements of the fast-ion distribution (invited). The Review of scientic instruments, **81**(10):10D727, October 2010.

[14]. M Salewski, B Geiger, D Moseev, W W Heidbrink, A S Jacobsen, S B Korsholm, F Leipold, J Madsen, S K Nielsen, J Rasmussen, and M Stejner. accepted, title = On velocity-space sensitivity of fast-ion D-alpha spectroscopy.

[15]. M. Salewski, S.K. Nielsen, H. Bindslev, V. Furtula, N.N. Gorelenkov, S.B. Korsholm, F. Leipold, F. Meo, P.K. Michelsen, D. Moseev, and M. Stejner. On velocity space interrogation regions of fast-ion collective Thomson scattering at ITER. Nuclear Fusion, **51**(8):083014, August 2011.

[16]. W. W. Heidbrink, R. E. Bell, Y. Luo, and W. Solomon. Fast-ion D-alpha diagnostic for NSTX. Review of Scientic Instruments, **77**(10):10F120, 2006.

[17]. B. Geiger, M. Garcia-Munoz, R. Dux, F. Ryter, G. Tardini, L. Barrera Orte, I.G.J. Classen, E. Fable, R. Fischer, V. Igochine, and R.M. McDermott. Fast-ion transport in the presence of magnetic reconnection induced by sawtooth oscillations in ASDEX Upgrade. Nuclear Fusion, **54**(2):022005, February 2014.

[18]. Y. Luo, W.W. Heidbrink, K.H. Burrell, D.H. Kaplan, and P. Gohil. Measurement of the D alpha spectrum produced by fast ions in DIII-D. The Review of scientic instruments, **78**(3):033505, March 2007.

[19]. M Podesta, W.W Heidbrink, R.E. Bell, and R. Feder. The NSTX fast-ion D-alpha diagnostic. The Review of Scientic Instruments, **79**(10):10E521, October 2008.

[20]. M a Van Zeeland, W.W Heidbrink, and J H Yu. Fast ion D imaging in the DIII-D tokamak. Plasma Physics and Controlled Fusion, **51**(5):1{19, May 2009.

[21]. M.a. Van Zeeland, J.H. Yu, W.W. Heidbrink, N.H. Brooks, K.H. Burrell, M.S. Chu, a.W. Hyatt, C. Muscatello, R. Nazikian, N.a. Pablant, D.C. Pace, W.M. Solomon, and M.R. Wade. Imaging key aspects of fast ion physics in the DIII-D tokamak. Nuclear Fusion, **50**(8):084002, August 2010.

[22]. A. Bortolon, W.W. Heidbrink, and M. Podesta. A tangentially viewing fast ion D-alpha diagnostic for NSTX. The Review of Scientic Instruments, **81**(10):10D728, October 2010.

[23]. WWHeidbrink, G.R McKee, D.R Smith, and a Bortolon. Beam-emission spectroscopy diagnostics also measure edge fast-ion light. Plasma Physics and Controlled Fusion, **53**(8):085007, August 2011.

[24]. C. a Michael, N. Conway, B. Crowley, O. Jones, W.W Heidbrink, S. Pinches, E. Braeken, R. Akers, C Challis, M Turnyanskiy, a Patel, D Muir, R. Gaka, and S. Bailey. Dual view FIDA measurements on MAST. Plasma Physics and Controlled Fusion, **55**(9):095007, September 2013.

[25]. M. Podesta, W. W. Heidbrink, D. Liu, E. Ruskov, R. E. Bell, D. S. Darrow, E. D. Fredrickson, N. N. Gorelenkov, G. J. Kramer, B. P. LeBlanc, S. S. Medley, a. L. Roquemore, N. a. Crocker, S. Kubota, and H. Yuh. Experimental studies on fast-ion transport by Alfven wave avalanches on the National Spherical Torus Experiment. Physics of Plasmas, **16**(5):056104, 2009.

[26]. M. Garcia-Munoz, I.G.J. Classen, B. Geiger, W.W. Heidbrink, M.a. Van Zeeland, S. Äkäslompolo, R. Bilato, V. Bobkov, M. Brambilla, G.D. Conway, S. Da Gra15ca, V. Igochine, Ph. Lauber, N. Luhmann, M. Maraschek, F. Meo, H. Park, M. Schneller, and G. Tardini. Fast-ion transport induced by Alfven eigenmodes in the ASDEX Upgrade tokamak. Nuclear Fusion, **51**(10):103013, October 2011.

[27]. B. Geiger, M. Garcia-Munoz, W.W. Heidbrink, R.M. McDermott, G. Tardini, R. Dux, R. Fischer, and V. Igochine. Fast-ion D-alpha measurements at ASDEX Upgrade. Plasma Physics and Controlled Fusion, **53**(6):065010, June 2011.

[28]. B. Geiger, R. Dux, R.M. McDermott, S. Potzel, M. Reich, F. Ryter, M. Weiland, D. Wünderlich, and M Garcia-Munoz. Multi-view fast-ion D-alpha spectroscopy diagnostic at ASDEX Upgrade. The Review of Scientic Instruments, **84**(11):113502, November 2013.

[29]. C M Muscatello, W W Heidbrink, Ya I Kolesnichenko, V V Lutsenko, M a Van Zeeland, and Yu V Yakovenko. Velocity-space studies of fast-ion transport at a sawtooth crash in neutral-beam heated plasmas. Plasma Physics and Controlled Fusion, **54**(2):025006, February 2012.

[30]. D.C. Pace, M.E. Austin, E.M. Bass, R.V. Budny, W.W. Heidbrink, J.C. Hillesheim, C.T. Holcomb, M. Gorelenkova, B. a. Grierson, D.C. McCune, G.R. McKee, C.M. Muscatello, J. M. Park, C.C. Petty, T.L. Rhodes, G.M. Staebler, T. Suzuki, M. a. Van Zeeland, R.E. Waltz, G. Wang, A.E. White, Z. Yan, X. Yuan, and Y. B. Zhu. Energetic ion transport by mmicroturbulence is insignicant in tokamaks. Physics of Plasmas, **20**(5):056108, 2013.

[31]. W.W. Heidbrink, Y. Luo, C.M. Muscatello, Y. Zhu, and K.H. Burrell. A new fast-ion D(alpha) diagnostic for DIII-D. The Review of Scientic Instruments, **79**(10):10E520, October 2008.

[32]. M. Salewski, B. Geiger, S.K. Nielsen, H. Bindslev, M. Garca-Muñoz, W.W. Heidbrink, S.B. Korsholm, F. Leipold, F. Meo, P.K. Michelsen, D. Moseev, M. Stejner, and G. Tardini. Tomography of fast-ion velocity-space distributions from synthetic CTS and FIDA measurements. Nuclear Fusion, **52**(10):103008, October 2012.

[33]. M. Salewski, B. Geiger, S.K. Nielsen, H. Bindslev, M. Garca-Mu~noz, W.W. Heidbrink, S.B. Korsholm, F. Leipold, J. Madsen, F. Meo, P.K. Michelsen, D. Moseev, M. Stejner, and G. Tardini. Combination of fast-ion diagnostics in velocity-space tomographies. Nuclear Fusion, **53**(6):063019, June 2013.

[34]. M. Salewski, B. Geiger, A.S. Jacobsen, M. Garca-Muñoz, W.W. Heidbrink, S.B. Korsholm, F. Leipold, J. Madsen, D. Moseev, S.K. Nielsen, J. Rasmussen, M. Stejner, G. Tardini, and M. Weiland. Measurement of a 2D fast-ion velocity distribution function by tomographic inversion of fast-ion D-alpha spectra. Nuclear Fusion, **54**(2):023005, February 2014.

[35]. H.-S Bosch and G.M Hale. Improved formulas for fusion cross-sections and thermal reactivities. Nuclear Fusion, **32**(4):611–631, April 1992.

[36]. H. Brysk. Fusion neutron energies and spectra. Plasma Physics, **15**:611–617, 1973.

[37]. J. Källne, L. Ballabio, J. Frenje, S. Conroy, G. Ericsson, M. Tardocchi, E. Traneus, and G. Gorini. Observation of the alpha particle "Knock-On" neutron emission from magnetically conned DT fusion plasmas. Physical Review Letters, **85**(6):1246–9, August 2000.

[38]. A. Pankin, D. McCune, R. Andre, G. Bateman, and A. Kritz. The tokamak Monte Carlo fast ion module NUBEAM in the National Transport Code Collaboration library. Computer Physics Communications, **159**(3):157–184, June 2004.

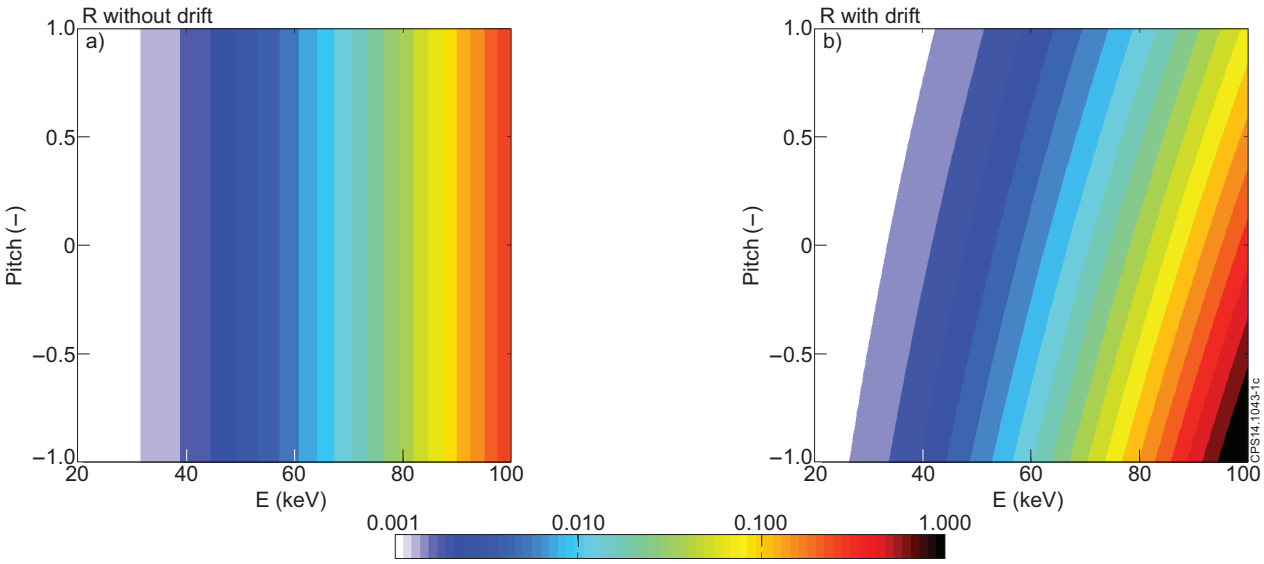

Figure 1: Rate functions with and without a drift of the target ions in units of $\left[\frac{N_n}{N_i s}\right]$. *The co-current drift velocity is 2.1* $\times 10^5 \frac{\mathrm{m}}{\mathrm{s}} m$ *. The thermal ion density is* $5 \times 10^{19} m^{-3}$.

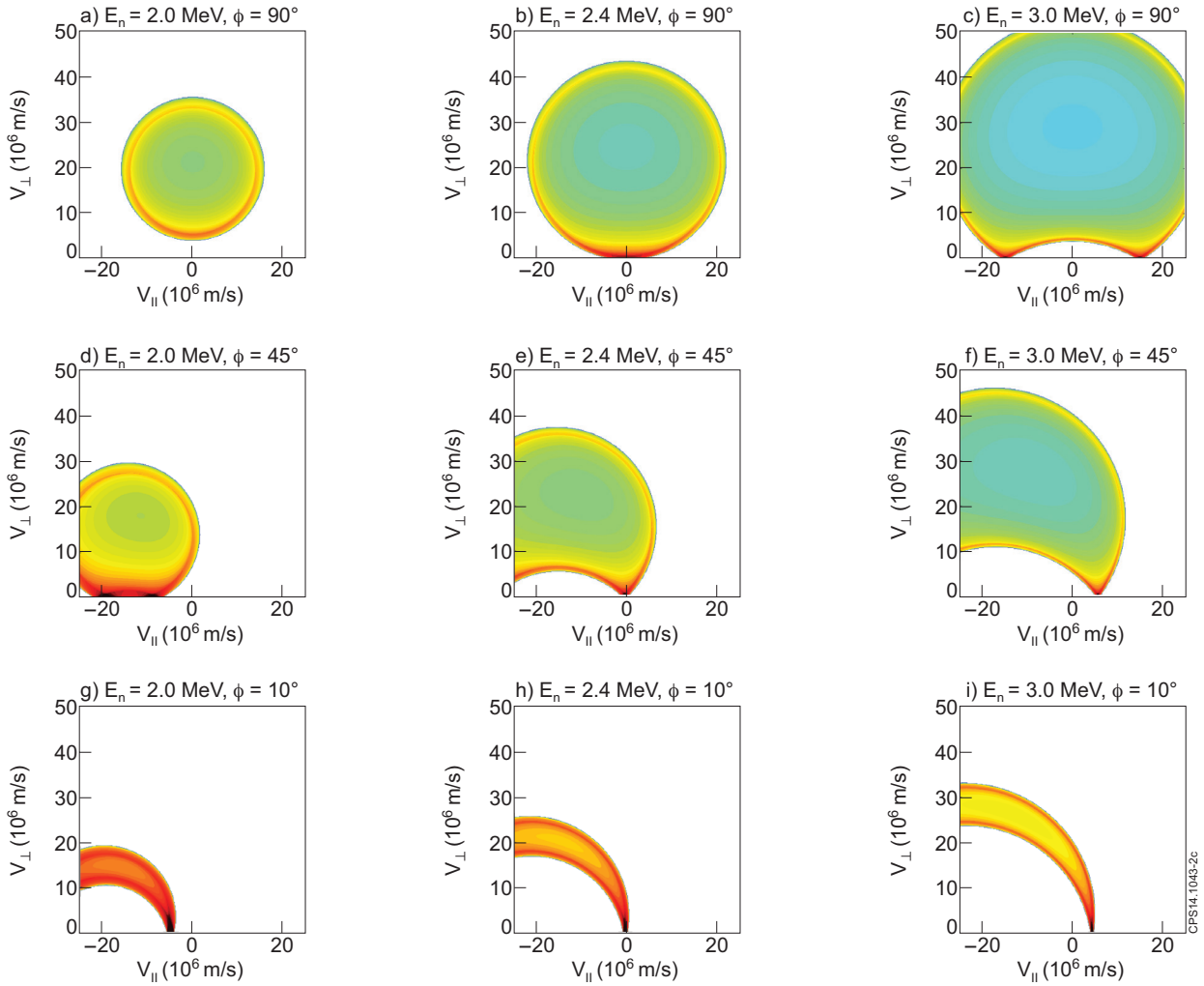

Figure 2: The probability part of neutron spectrometry weight functions calculated in $(v_{//}, v_{\perp})$*-space for* $\Delta E_n = 0.1 MeV$ *centered at* E_n.

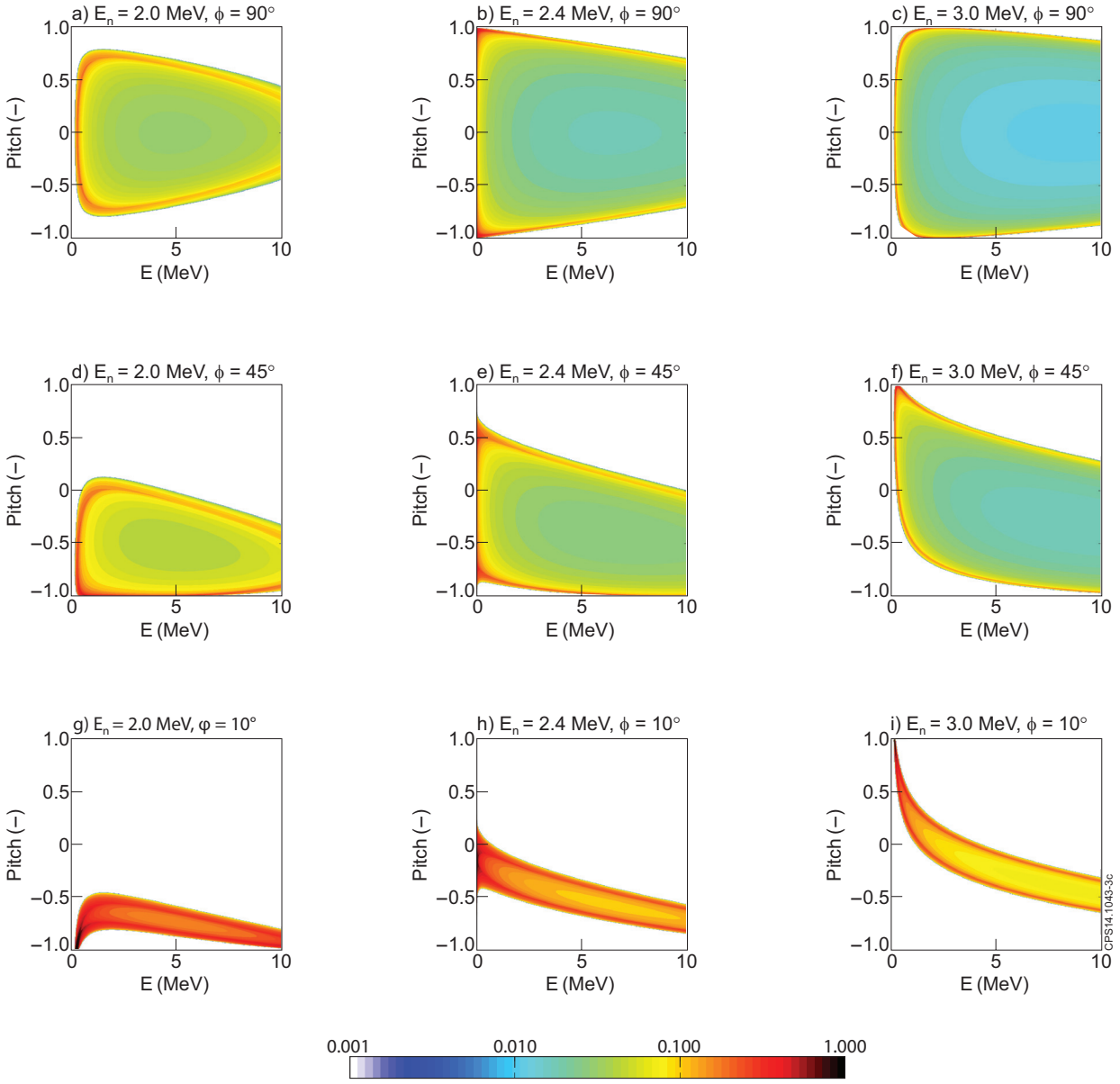

Figure 3: The probablity part of neutron spectrometry weight functions calculated in (E, p)-space for ΔE_n = 0.1MeV centered at E_n.

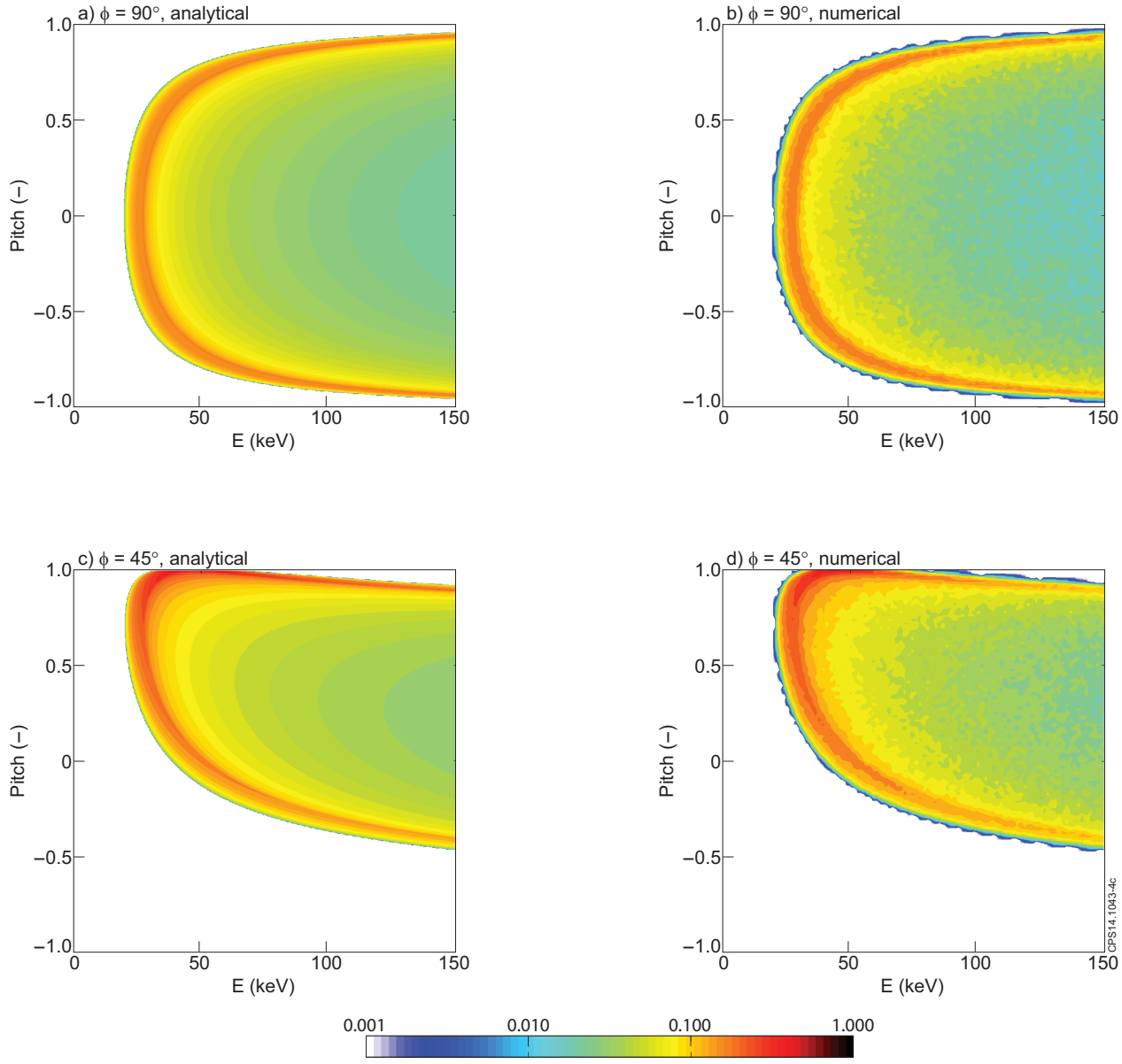

Figure 4: Comparison of the probability part of neutron spectrometry weight functions calculated numerically and analytically, for E_n = 2.6MeV and ΔE_n = 0.03MeV.

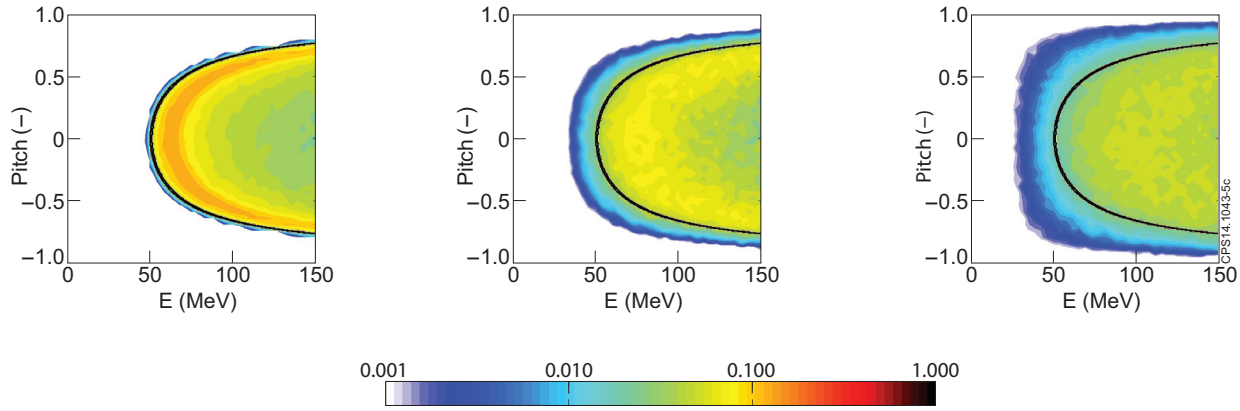

Figure 5: Probability part of neutron spectrometry weight functions with $\phi = 90°$, $E_n = 2.2MeV$ and $\Delta E_n = 0.03MeV$ calculated for various thermal ion temperatures. The thick black lines show the edge of the T = 0 weight functions.

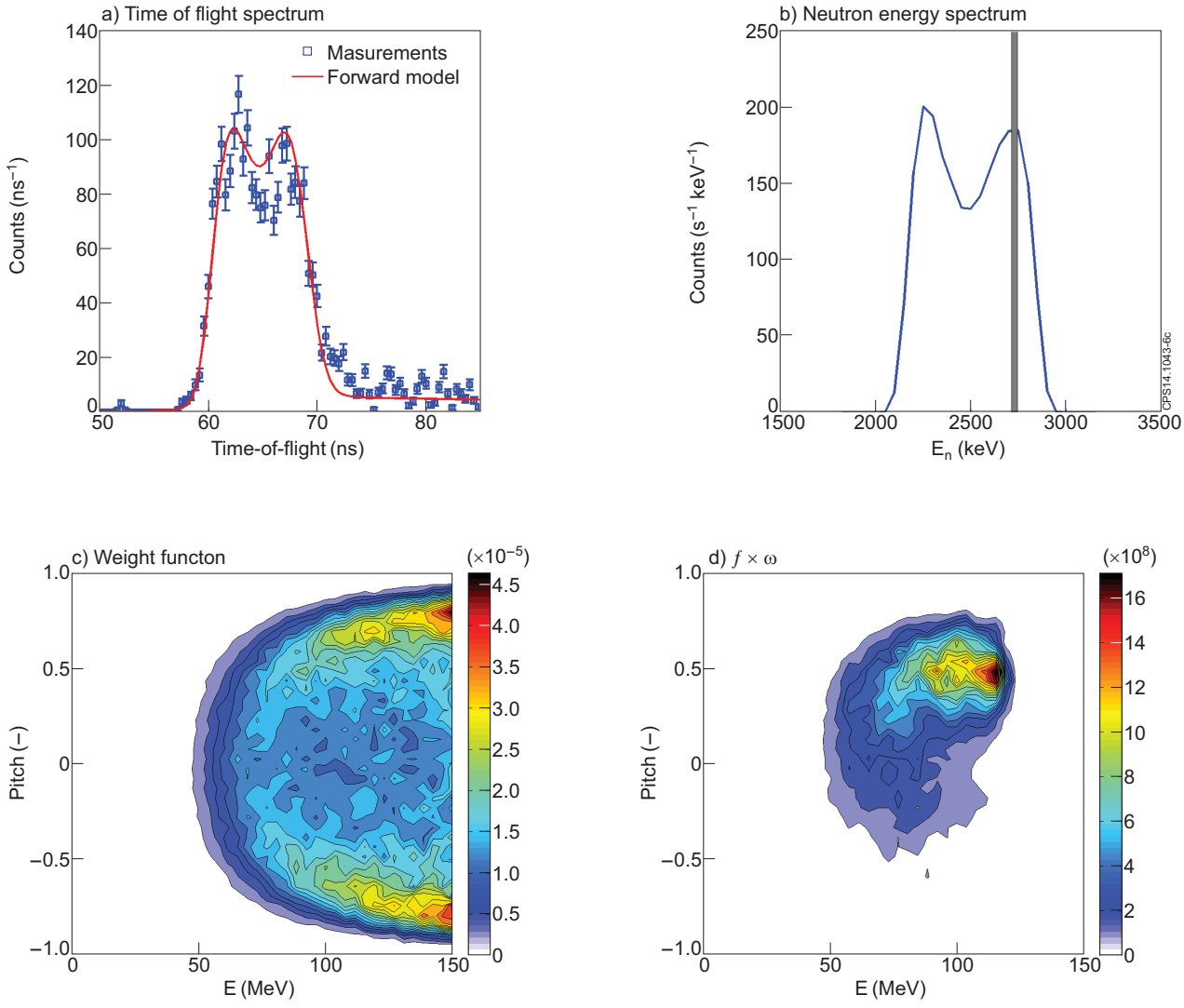

Figure 6: Example of applying the weight function approach to neutron measurements at JET.

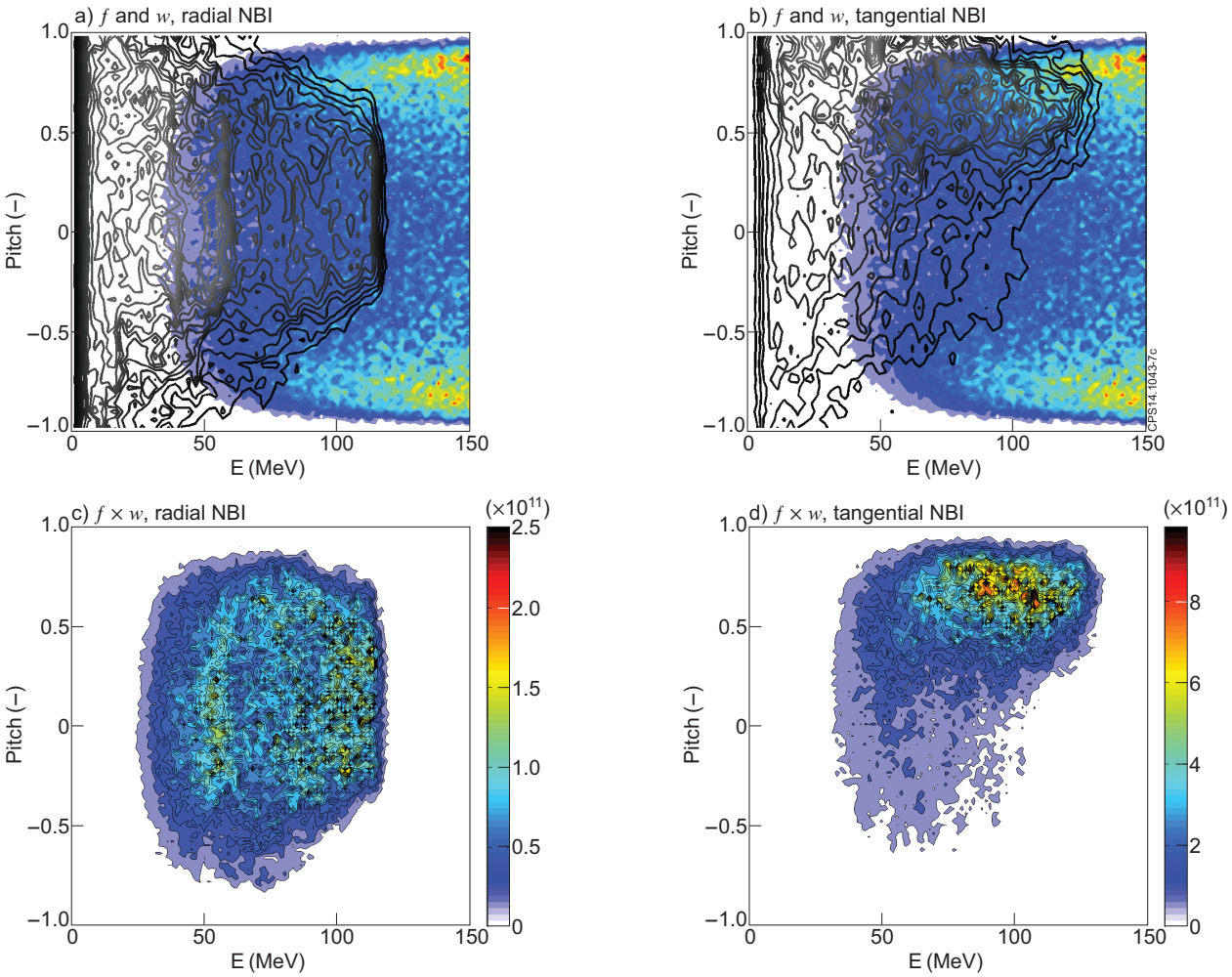

Figure 7: (a-b) By plotting a calculated distribution function together with a calculated weight function, it is possible to visualize the region in velocity space which is accessible by a given part of the neutron energy spectrum. (c-d) shows the product of f and w, which illustrates where most neutrons come from, given the calculated distribution function. These examples are for a numerical weight function calculated for $E_n = 2.3 \pm 0.015$MeV and $\phi = 90°$. The distribution functions are calculated for JET Pulse Number: 69242 using TRANSP together with the NUBEAM module.

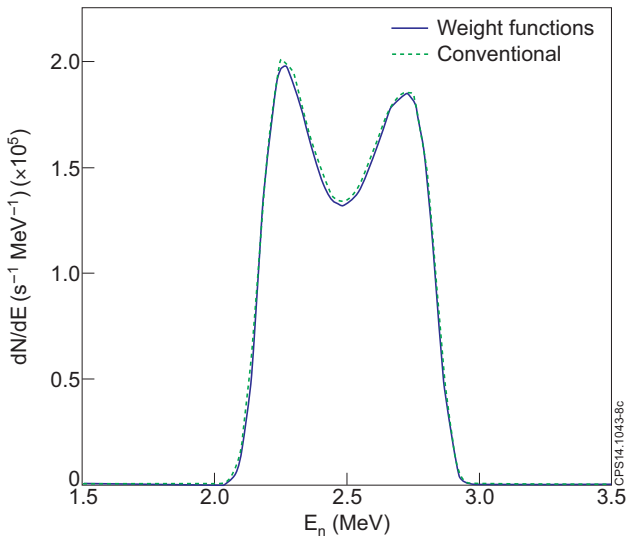

Figure 8: Comparison of a spectrum computed using a fast forward-model based on weight functions, and a spectrum calculated using the conventional forward model calculated using a Monte Carlo approach.